Using the dGEMRIC technique to evaluate cartilage health in the presence of surgical hardware at 3T: comparison of inversion recovery and saturation recovery approaches

Authors

Agnes G. d'Entremont, MASc[1,2] (agnes.dentremont@gmail.com)

Shannon H. Kolind, PhD[3] (skolind@alumni.uvic.ca)

Burkhard Mädler, PhD[4] (burkhard.maedler@ukb.uni-bonn.de)

David R. Wilson, DPhil[2,5] (david.wilson@ubc.ca)

Alexander L. MacKay, DPhil[6] (mackay@physics.ubc.ca)

Affiliations

[1] Department of Mechanical Engineering, University of British Columbia

[2] Centre for Hip Health and Mobility, University of British Columbia

[3] Institute of Psychiatry, University of British Columbia

[4] Department of Neurosurgery, Friedrich-Wilhem's University, Bonn, Germany

[5] Department of Orthopaedics, University of British Columbia

[6] Department of Physics and Astronomy, University of British Columbia

Corresponding author

Agnes G. d'Entremont

Department of Orthopaedics, University of British Columbia 910 West 10th Avenue, Room 3114, Vancouver, BC V5Z 4E3 Canada

Phone: 604 739 0029

Fax: 604 675 2576

Email: agnes.dentremont@gmail.com

Supported by the Canadian Institutes of Health Research, Operating Grant MOP-106680

Running title

dGEMRIC and metal artifact at 3T

Using the dGEMRIC technique to evaluate cartilage health in the presence of surgical hardware at 3T: comparison of inversion recovery and saturation recovery approaches

Abstract

Objective. To evaluate the effect of metal artifact reduction techniques on dGEMRIC T_1 calculation with surgical hardware present.

Materials and Methods. We examined the effect of stainless steel and titanium hardware on dGEMRIC T_1 maps. We tested two strategies to reduce metal artifact in dGEMRIC: 1) saturation recovery (SR) instead of inversion recovery (IR) and 2) applying the Metal Artifact Reduction Sequence (MARS), in a gadolinium-doped agarose gel phantom and *in vivo* with titanium hardware. T_1 maps were obtained using custom curve-fitting software and phantom ROIs were defined to compare conditions (metal, MARS, IR, SR).

Results. A large area of artifact appeared in phantom IR images with metal when TI≤700ms. IR maps with metal had additional artifact both *in vivo* and in the phantom (shifted null points, increased mean T_1 (+151% IR ROIartifact) and decreased mean inversion efficiency (f; 0.45 ROIartifact, versus 2 for perfect inversion)) compared to the SR maps (ROIartifact: +13% T_1 SR, 0.95 versus 1 for perfect excitation), however SR produced noisier T_1 maps than IR (phantom SNR: 118 SR, 212 IR). MARS subtly reduced the extent of artifact in the phantom (IR and SR).

Conclusion. dGEMRIC measurement in the presence of surgical hardware at 3T is possible with appropriately applied strategies. Measurements may work best in the presence of titanium and are severely limited with stainless steel. For regions near hardware where IR produces large artifacts making dGEMRIC analysis impossible, SR-MARS may allow dGEMRIC measurements. The position and size of the IR artifact is variable, and must be assessed for each implant/imaging set-up.

Keywords

Metal artifact; dGEMRIC; knee; cartilage; surgical implant; magnetic resonance imaging

Introduction

Osteoarthritis (OA), or injury associated with development of OA such as a ligament tear, is sometimes treated with surgery with the objective of slowing, arresting, or preventing cartilage degeneration. Sensitive, non-invasive evaluations of cartilage degeneration are important for making objective assessments of how effectively surgical treatments achieve these objectives.

Delayed Gadolinium-Enhanced MRI of Cartilage (dGEMRIC) is a non-invasive imaging method that measures a surrogate for glycosaminoglycan (GAG) concentration in articular cartilage[1]. GAG is a macromolecule whose concentration is directly related to the mechanical stiffness of cartilage[2]. Prior to the development of dGEMRIC, GAG could only be assessed histologically. To perform the dGEMRIC procedure[3], anionic gadolinium contrast agent (Gd-DTPA^{2-}) is first injected intravenously or intraarticularly and then allowed to diffuse into the cartilage during a prescribed wait time. The contrast agent distributes in inverse proportion to the GAG content due to Coulomb interaction (because both are negatively charged), and causes a local change in T_1. The concentration of GAG in cartilage can then be estimated by calculating the reduction of the longitudinal relaxation time T_1 after Gd-administration from appropriate MR images of the cartilage. dGEMRIC has been validated[1] and used at the knee to study several populations cross-sectionally including patients with autologous chondrocyte transplants[4,5], subjects with differing physical activity levels[6,7], subjects with knee malalignment[8], subjects with ACL injury and/or subsequent repair[9,10], and subjects with OA or OA risk factors[7–9,11,12]. Only a few studies and case reports have followed subjects longitudinally[7,13–16].

While there are a number of potential applications for dGEMRIC imaging near surgical hardware, it is not clear to what extent implanted surgical hardware affects the T_1 measurements that are used to infer GAG concentration in dGEMRIC imaging. In one study of high tibial osteotomy which used dGEMRIC with substantial surgical hardware in place, the authors did not address the effect of metal artifact on their results[15]. Another group recommended that implants be removed prior to dGEMRIC imaging, however that requirement may significantly limit applications in regions where hardware removal is not standard clinical practice[16], or where it is not possible. The effect of metal on T_1 measurements is of particular concern in high-field MR systems (3T), which offer a superior signal-to-noise ratio with increased spatial resolution and are therefore preferable to investigate thin structures like knee cartilage, but produce higher static field (B_0) and radio frequency field (B_1) inhomogeneity artifacts in the presence of metal implants. Several types of metal artifact reduction techniques exist: one such approach for B_0 artifacts is the Metal Artifact Reduction Sequence (MARS). MARS has been developed and utilized for clinical applications[17–20], but its effect on a quantitative imaging method such as dGEMRIC has not been determined.

Our objectives for this study were to assess and optimize the dGEMRIC procedure in the presence of surgical hardware for high-field (3T) clinical MR systems. The following questions are addressed in this study: Can the conventional dGEMRIC method using inversion recovery (IR) be used near stainless steel and/or titanium implants without modification? What are the effects on T_1 maps of using IR, saturation recovery (SR) and/or MARS in a phantom with and without metal? What are the effects of using IR, SR and/or MARS *in vivo*?

Methods

Initial testing was done *in vivo* to determine whether high tibial osteotomy plates of different materials caused artifact through the cartilage. Then, the extent of this artifact and the effects of techniques to reduce it were explored using a gadolinium-doped phantom. These techniques were assessed *in vivo* in human subjects with implanted high tibial osteotomy plates. Finally, simulations were used to further explore the effect of changes in signal-to-noise ratio (SNR) on the results.

Initial in vivo testing

To initially, qualitatively assess the presence and severity of artifact in images and T_1 maps due to titanium and stainless steel high tibial osteotomy plates, we performed dGEMRIC scans following a procedure based on a published, established protocol[1] on the knee joint cartilage of two human subjects with implanted metal plates. One subject (female, age 49, 4 months post-op) had a stainless steel Puddu plate (Arthrex, Naples, Florida) in the proximal tibia from a high tibial osteotomy operation and the other subject (female, age 40, 14 months post-op) had a titanium Small Fragment plate (Synthes, West Chester, Pennsylvania)) from a high tibial osteotomy. In both cases, the indication for surgery was medial tibiofemoral OA caused by varus knee malalignment. The study received approval by our Clinical Research Ethics Board and informed consent was obtained.

Each subject was injected with a double dose (0.2 mmol/kg) of gadopentatate dimeglumine (Gd-DTPA^{2-}, Magnevist, Berlex Laboratories, USA). Subjects performed ten minutes of brisk walking following the injection and scanning began 90 minutes post-injection. We performed a series of single-slice inversion recovery fast spin-echo (FSE) scans (IR) on each subject's operated knee (tibiofemoral (TF) joint, coronal plane) using

a Philips 3T Achieva scanner, with two surface coils (SENSE Flex-M, Philips, Best, Netherlands) positioned with one on either side of the joint (Table 1). These coils were the best available at the scanner for knee use at the time of the study. The inversion preparation was achieved with a commercially available hyperbolic secant adiabatic pulse (amplitude and frequency modulated) which was designed to produce accurate inversion pulses even in presence of radiofrequency field (B_1) inhomogeneities[21].

Phantom studies

Next, we tested two strategies to reduce metal artifacts in phantoms: 1) using saturation recovery fast spin-echo (SR) instead of IR and 2) applying the Metal Artifact Reduction Sequence (MARS) to both types of series (IR and SR). SR sequences have been used with dGEMRIC in the literature[2,22], though less frequently than IR sequences[1]. MARS is based upon view-angle tilting (VAT)[23] with an increased read bandwidth (from +/- 26.9 kHz to +/- 46.0 kHz) to combat the blurring associated with VAT. The same IR and SR series were used with and without the addition of MARS (no change in imaging time; Table 1).

These strategies were first tested on two gadolinium-doped phantoms designed to simulate T_1 values of cartilage containing contrast agent. One phantom included a titanium HTO plate and four screws (Arthrex Puddu plate, Ti6Al4V, approximately 5 cm x 1.5 cm) placed inside the container with an orientation in the B_0 field similar to that of an implanted plate imaged *in vivo*. Each phantom consisted of a plastic container, filled with 1% agarose gel (Bio Rad, Hercules, CA; prepared with distilled water) doped with 0.3 mM Gd-DTPA^{2-}(Figure 1(a)). This concentration was chosen to obtain a T_1 value for the phantom of around 500 ms at 3T. We scanned the phantom using the standard dGEMRIC protocol described above (IR) as well as with a modified protocol using a

single-slice saturation recovery (SR) sequence in the coronal plane (Table 1). The SR method was chosen for its easy implementation and relative insensitivity to B_0 and B_1 inhomogeneities as compared to faster spoiled gradient echo methods with variable flip angle for T_1 measurement. MARS was applied to each series (IR and SR), and all four protocols (IR, SR, IR-MARS, SR-MARS) were used to image the phantom (Table 1).

Agarose gel was chosen as a phantom material because there appeared to be vibration artifacts in the SR images when saline was used. A saline based-phantom was also imaged with the same scan parameters. Although the analysis will not be presented, we have included an image to show differences in artifact with phantom material (Figure 1(c)).

In vivo studies

The effect of different pulse sequences on metal artifact in dGEMRIC scans was assessed *in vivo*. To assess the effect of SR versus IR on artifact reduction *in vivo*, one subject (male, age 60, 6 months post-op) with a titanium Arthrex Puddu plate from a high tibial osteotomy surgery was scanned at both the patellofemoral (PF) and tibiofemoral (TF) joints (axial and coronal slices, respectively) using SR and IR at each joint (Table 1). Clinical Research Ethics Board approval for the study and informed consent were obtained. Since the patellofemoral joint was far enough away from the implant to have no visible artifact, this joint was used to directly compare the two sequences *in vivo*. Scanning was performed over two sessions two days apart, because the contrast dwell time in cartilage following injection was not long enough to complete all four scans in one session. Selection of imaging planes was made with reference to previous scans. Because contrast agent diffuses more quickly into thinner cartilage, at each session the thinner cartilage of the tibiofemoral joint was imaged first, followed by the thicker

patellofemoral cartilage. Sequences were identical to those used in the previous *in vivo* and phantom scanning.

To assess the effect of MARS on artifact reduction *in vivo*, the same subject was scanned at the tibiofemoral joint (coronal slice) with and without MARS and using an SR series (SR and SR-MARS). This scanning was performed eleven months following the above-mentioned scans, when MARS became available, to compare to the data already collected.

Curve fitting for T_1 calculation

Quantitative T_1 maps were obtained using in-house developed code (MATLAB, Mathworks, MA, USA, function lsqcurvefit) to fit the magnitude signal intensities versus inversion times and repetition times respectively for each pixel of the image series. The *in vivo* images were manually registered and cartilage was segmented by one experienced observer. Since the phantom was not moved between any of the images there was no need to register these images.

$$SI = \left| S_0 \left(1 - f_{IR} e^{-\frac{TI}{T_1}}\right) \right|$$

Equation 1

$$SI = S_0 \left(1 - f_{SR} e^{-\frac{TR}{T_1}}\right)$$

Equation 2

Equation 1 is the fit equation for the IR series, and Equation 2 is the fit equation for the SR series. SI is signal intensity in the image, S_0 is the signal intensity at equilibrium conditions, TI is inversion time, TR is repetition time and f_{IR} and f_{SR} are fit factors that account for imperfect inversion and slice excitation flip angles (f_{IR} = 2 for perfect

inversion, f_{SR} = 1 for perfect excitation). SI, TI, and TR are known values, and S_0, T_1 and f are calculated.

Twenty-five random initial values sets, centered around initial guesses (IR: $T_{1,initial}$ = $TI(SI_{min})/ln2$, $S_{0,initial}$ = $SI(TI_{max})$, $f_{IR,initial}$ = 2; SR: $T_{1,initial}$ = 500 ms, $S_{0,initial}$ = $SI(TR_{max})$, $f_{SR,initial}$ = 1) were used for each voxel and the result with the lowest residual was selected as the best result. Bounds for IR were: T_1 = 0 to 3500 ms, S_0 = 0 to 300, f_{IR} = 0 to 2. Bounds for SR were: T_1 = 0 to 3500 ms, S_0 = 0 to 300, f_{SR} = 0 to 1. Initial work showed large differences in calculated T_1 in IR artifact areas when the lower bounds for f_{IR} were changed from 1 to 0. .

The calculated T_1 maps from both phantom and *in vivo* images contained pixel values that were obviously outliers, especially in the presence of metal or increased noise in the signal. Since the physiological range of mean post-contrast T_1 (both normal and OA) has been found to be 400-900 ms[24] we chose to conservatively remove pixels above 1200 ms and below 100 ms from all data sets.

For the phantom, four regions of interest (ROI) of 900 pixels each (about the same number as in the cartilage area) were defined: one was located in the approximate region where one would expect to find cartilage with respect to the superior screw *in vivo*, as determined from relative position on *in vivo* images ($ROI_{cartilage}$), two were located at the superior and inferior edges of the image (ROI_{away1} and ROI_{away2}), and one was chosen to cross the large artifact visible in IR maps and lower TI images ($ROI_{artifact}$)(Figure 1). Calculated T_1 values were separated into 10 ms bins and histograms of these bins were created and compared.

Effect of noise on curve fitting

To investigate the effect of noise level on the resulting calculated T_1 value, simulations of both IR and SR measurements were performed using MATLAB (Mathworks, MA, USA). Base data sets for both IR and SR were created using equations 1 and 2 respectively, with values of T_1, S_0 and f chosen to match the IR and SR 'no metal, no MARS' phantom values (IR: $T_{1,initial}$ = 570, $S_{0,initial}$ =41 $f_{IR,initial}$ = 1.870; SR: $T_{1,initial}$ = 537, $S_{0,initial}$ =41 $f_{SR,initial}$ = 0.987) and the same TIs and TRs used in the IR and SR imaging respectively (Table 1).

Random normally distributed noise vectors of a given standard deviation (or signal to noise ratio (SNR)) were added to the base data sets (SR(real), SR(imaginary), IR(real) and IR(imaginary)) to create noisy data sets. The magnitude of the complex noisy data was calculated from real and imaginary values to obtain IR(magnitude) and SR(magnitude), which is equivalent to data output by the scanner (i.e. Rician noise). Both noisy data sets, SR(magnitude) and IR(magnitude), were then fit using the appropriate equation and a least squares fit (MATLAB function lsqcurvefit). Twenty-five random initial values sets, centered around the nominal values, were used for each noisy data set and the result with the lowest residual was selected as the best result. The noise addition and fit were repeated 900 times at each noise level for each measurement type, and the resulting T_1 values were averaged.

SNR was estimated from phantom and *in vivo* T_1 maps as the ratio between calculated signal intensity at equilibrium (S_0) and the mean residual (absolute value), for each pixel in the map. Pixel SNR values were then averaged over the ROI.

Statistical analysis

Summary statistics were performed for the phantom overall, for each ROI, and for the noise simulation. In each phantom ROI or tissue ROI, we tested the null hypothesis that

mean T_1 values were the same between sequences and metal conditions (for example, in $ROI_{cartilage}$, between IR without metal and IR with metal, IR without metal and IR-MARS without metal, IR without metal and SR without metal, etc.) using the Student's t-test with Bonferroni correction ($alpha_{Bonferroni}$ = 0.00067; MATLAB, Mathworks, MA, USA).

Results

Initial in vivo testing

Our initial *in vivo* images showed that it is not possible to obtain accurate dGEMRIC scores in tibial cartilage after implantation of either stainless steel or titanium osteotomy plates using our conventional IR sequence. Images from the subject with a stainless steel plate implanted in the proximal tibia could not be used for dGEMRIC analysis due to distortion from the plate (Figure 2, left). Images from the subject with a titanium plate implanted in the proximal tibia exhibited much less distortion (Figure 2, center). The cartilage area, in particular, appeared unaffected. However, many of the signal intensity versus T_1 time curves for single pixels in the cartilage areas did not show the typical null point in a standard IR-curve and were often nearly flat (Figure 2, below right). Consequently calculated T_1-values from these regions were unreliable. When mapped, the calculated T_1 values showed large variations across the cartilage plate, and there was a clear demarcation in the medial tibiofemoral cartilage (Figure 2, right, white arrow).

Phantom studies

Compared with the IR images, we observed much less distortion of T_1 when using the SR series on the same phantom with a titanium plate in the same location (Figure 3). However, the SR series resulted in a noisier image than the IR series because of a lower intrinsic signal-to-noise ratio in the basis images and the absence of the characteristic

null-point to aid in curve fitting, which may preclude finding small differences in T_1. MARS subtly reduced the extent of the artifact in the IR-MARS map (see lower right edge of map, for example), and in the SR-MARS map (improvement may be seen at the lower screw, for example) (Figure 3).

The effect of metal on $ROI_{artifact}$ was dramatic: because so many of the IR and IR-MARS values were excluded as outliers, data for $ROI_{artifact}$ both with and without outliers is presented (Table 2). Adding metal resulted in an increased T_1 in IR and IR-MARS (14% and 0.5% respectively); including the outliers, the increases were much larger (151% IR and 135% IR-MARS). The mean f_{IR} values in $ROI_{artifact}$ with metal were 0.45 (IR) and 0.41 (IR-MARS), compared to a nominal value of f_{IR} = 2 (Figure 4). For SR, adding metal increased mean T_1 values (+13% SR, +7% SR-MARS), with no substantial difference when outliers were included (Table 2). The values of f_{SR} were 0.95 (SR) and 0.96 (SR-MARS) in $ROI_{artifact}$, compared to a nominal value of f_{SR} = 1, and SR f-maps showed a smaller extent of artifact than T_1 maps (Figure 4). Maps of M_0 values showed similar distortion in IR and SR, but did not show the additional area of IR artifact seen in T_1- and f-maps (Figure 4). When outliers are considered, the sequence that best recovered $ROI_{artifact}$ 'no metal' values was SR-MARS (+6.8%).

For the cartilage region of interest in the phantom ($ROI_{cartilage}$), adding metal had a slightly larger effect on the mean T_1 for the SR sequence than for IR (+11% IR, +18% SR). Adding metal had a slightly larger effect on the standard deviation of T_1 for the IR sequence than for SR (+34 ms IR, +30 ms SR). Both IR-MARS and SR-MARS gave rise to similarly recovered $ROI_{cartilage}$ T_1 values without metal (+10.1% and +10.5% from original), partly due to the reduction in extent of artifact such that it intruded less into $ROI_{cartilage}$ (Figure 3, Table 2).

In the small ROIs, there were no outliers in $ROI_{cartilage}$, ROI_{away1} or ROI_{away2} for any condition. For $ROI_{artifact}$, outliers in the metal condition for IR (39% of pixels) and IR-MARS (41% of pixels) were primarily T_1 values above 1200 ms (99.7% and 86.1% of outliers respectively), while for SR outliers were all above 1200 ms (0.4% of pixels).

The overall mean T_1 value for the SR sequence (without metal or MARS) was 31 ms (5%) lower ($p < 0.00067$, $alpha_{Bonferroni} = 0.00067$) than the IR result (Table 2). Adding MARS (without metal) changed the overall mean T_1 by -0.2% (IR, $p < 0.00067$) and +2.2% (SR, $p < 0.00067$) and increased the standard deviation minimally (average of 3 ms) (Table 2, Figure 5).

MARS resulted in statistically significant different T_1 values for the overall image using IR (without metal only) and SR (both with and without metal), although the absolute differences were small (under 2%, or 11.7 ms, in each case). No statistical differences in T_1 were found between the standard and MARS sequences for the following ROIs and sequences: the overall image: IR with metal (outliers excluded, $p = 0.46$); $ROI_{cartilage}$: IR without metal ($p = 0.55$); ROI_{away2}: IR with metal ($p = 0.10$); and $ROI_{artifact}$: IR without metal ($p = 0.76$), SR without metal ($p = 0.00074$), IR with metal (outliers included, $p = 0.10$). There was no statistical difference in T_1 between IR and SR for: ROI_{away2} with metal ($p = 0.03$); or between IR-MARS and SR-MARS for: $ROI_{cartilage}$ with metal ($p = 0.003$), $ROI_{artifact}$ with metal (outliers excluded, $p = 0.27$). For $ROI_{artifact}$, no difference in T_1 was found between IR without metal and IR-MARS with metal (outliers excluded, $p = 0.70$); or in IR-MARS between metal and no metal conditions (outliers excluded, $p = 0.69$). All other comparisons between sequences within ROIs were significantly different ($p < 0.00067$).

IR and SR phantom histogram results show similar ranges in T_1 without MARS or metal (Figure 5). Adding MARS without metal resulted in similar T_1 values for both IR and SR. Adding metal resulted in a greater spread of values (including a number of low outliers for IR and high outliers (not plotted) for IR and SR) and a shift of the peak to higher T_1 values for both IR and SR. When MARS was added, the IR-MARS T_1 histogram stayed about the same but the SR-MARS histogram spread further and the peak shifted toward the 'no metal' mean (Figure 5).

A large area of artifact was evident in the IR images with metal where TI was 700 ms or less (Figure 6). For a line of adjacent pixels crossing into the artifact, the null point of the measured inversion curve shifted left, implying a shorter and shorter T_1 within the homogeneous phantom (Figure 6, right). About six pixels (approximately 2.3 mm) into the artifact from the boundary of the distortion, the null point shifted below 50 ms (our lowest TI value), and the curves were similar to those from the preliminary *in vivo* subject with titanium. The effect on the T_1 map was an area of substantially decreased and consequently inaccurate T_1 values (Figure 3). In these areas, f_{IR} was often quite low, at or below 1.

In vivo studies

In the patellofemoral (PF) joint images (axial), the mean value of T_1 for SR was 9% higher than for IR ($p < 0.00067$) (Table 2, Figure 7). The SR series had a 33% higher standard deviation. In the IR and SR PF scans, outliers excluded by the 100-1200 ms range were on average 0.5% of all pixels. There was no visible artifact in the PF images, or any indication of artifact in the T_1, f or M_0 maps. Since there was no artifact detectable

in the PF images (Figure 7), the testing of the MARS sequence was limited to the tibiofemoral (TF) images (coronal).

In the tibiofemoral (TF) maps, the mean value of T_1 for SR was 12% higher than for IR (significantly different, $p < 0.00067$) (Figure 7). Mean SR-MARS T_1 was 7% lower than mean SR T_1 ($p < 0.00067$) at the same timepoint. Due to the nearly complete loss of cartilage in the subject's medial tibiofemoral compartment associated with varus malalignment, only the lateral compartment was considered. Outliers excluded by the 100-1200 ms range in the tibiofemoral joint were an average of 6% of pixels in ROIs over all TF maps. Mean translation for all *in vivo* images for registration was 0.34 pixels.

There were clear artifacts in the TF images below the cartilage region, however it was not clear how far the artifact extended. The TF IR single pixel curves and f-factor map show that the artifact extended into the cartilage of the tibial plateau (shift of null point below 50 ms and f-factor values below 1) (Figure 7).

Effect of noise on curve fitting

The averaged T_1 values calculated from the simulated base data sets without noise were 570 ms (IR) and 537 ms (SR), as expected since these were the input numbers (Table 3). As noise was added the calculated T_1 values obtained from the IR simulation decreased slightly (to T_1 = 561 ms at SNR = 20) and then increased (605 ms at SNR = 5), while the T_1 values from the SR simulation increased from 537 ms as noise increased (T_1 = 570 ms at SNR = 20, T_1 = 714 ms at SNR = 5).

Estimates of average SNR for phantom ROIs (no metal, no MARS) were 212 (SD 81) for IR, and 118 (SD 42) for SR. For *in vivo* PF images, estimates of average SNR in the cartilage were 38 (SD 22) for IR, and 30 (SD 14) for SR.

Discussion

We assessed methods for reducing metal artifact in the dGEMRIC procedure because there are many applications for dGEMRIC in joints with implanted surgical hardware. We found that artifact in the T_1 map may be present with titanium hardware, even if the high TI images do not appear distorted, and that using SR instead of IR can significantly reduce artifacts in the T_1 map. We found that dGEMRIC imaging near stainless steel implants is not possible, and that the addition of MARS can reduce T_1 map artifact somewhat. This paper is focused on one particular surgery and surgical implant, however the methods and strategies presented would be similar for the evaluation of any joint and implant.

Our results show that artifacts from metal can disrupt T_1 measurements in a clinically relevant situation, particularly when using IR sequences. The pattern of the IR artifact varied greatly with phantom material (Figure 1), and IR artifact was also apparent in the cartilage *in vivo* (Figure 2, Figure 7: TF IR). The effect of the IR artifact in the phantom was typically to increase the calculated T_1 value when the f-factor was allowed to vary widely (when the f-factor was narrowly bounded in IR artifact areas, fits were poor and T_1 values varied). In the IR artifact areas, both *in vivo* and in the phantom, the null point of the curve shifted below our lowest TI value, indicating that the IR pulse was close to 90 degrees. The effect of this was observable in alteration of the IR f-maps (Figure 4). Because the artifact depends on multiple factors, the extent of artifact is particular to a type of surgery and type of implant, and even orientation in the main magnetic field. To

determine if the artifact will extend into cartilage, each type of surgery and imaging set-up must be considered individually.

It is not surprising that MARS does not completely eliminate metal artifacts. MARS corrects mis-mapping due to B_0 inhomogeneity in the imaging plane, but does not affect other metal artifacts, while the SR sequence is more robust in the presence of B_1 inhomogeneity. Metal affects both the B_0 and B_1 fields and generally causes degradation in MR images due to a variety of artifacts. Off-resonance artifacts are caused by alterations in the local magnetic field that cause spins to be mapped to the wrong spatial location due to B_0 radiofrequency field inhomogeneity, while B_1 field inhomogeneities lead to imperfect 180 degree pulses near the metal which changes the nature of the experiment such that the standard curve fitting equation is invalid. The location and severity of these artifacts depends on the pulse sequence and imaging parameters[25,26], as well as other factors that one has less control over such as the type of metal[27–29], orientation of implant in the main magnetic field[27,28] and field strength[27,28,30]. Our finding that images with stainless steel implants were much more distorted than those with titanium implants is consistent with results in the literature[29].

MARS produced a small improvement to the extent of artifact in the phantom, however even a small reduction in extent of artifact may increase the possibility of obtaining dGEMRIC results in an important area of cartilage. For example, in the phantom maps with metal, MARS reduced the artifact extent such that it extended less within $ROI_{cartilage}$ for both IR and SR. Similarly, in the *in vivo* comparison SR-MARS reduced the area of artifact in the overall TF images compared to SR, although it was more difficult to evaluate the extent of artifact in the TF cartilage area.

Differences in T_1 values with sequence where no metal was present (5% 'no metal' phantom, 9% PF *in vivo*) are not adequately explained by SNR factors. As our simulations demonstrated, the curve fitting for SR is less robust in the presence of noise, and increased noise leads to increased T_1 values while the IR curve fitting is more stable in the presence of noise. As was seen in the estimates of SNR from images, SR is noisier than IR in practical usage and *in vivo* images are noisier than phantom images (due to differences in tuning, flow artifacts, and subject movement), and therefore the effect may be compounded when using SR *in vivo*, where we observed that IR T_1 values tended to be smaller than SR T_1 values without metal artifact. However, the phantom condition results without metal exhibited the opposite pattern, where IR T_1 values were found to be larger than SR results. It is not clear what other factors may be involved in the differences between experimental values of T_1 measured with IR and SR without metal. Since the value of T_1 depends only on tissue and field strength, the observed differences in T_1 between IR and SR measurements are likely functions of the curve fits and/or the sequences themselves rather than real differences in T_1. The effect of limited repetition time on the IR phantom experiment was probed by including an additional fit term (+ $e^{-TR/T1}$) in the equation, however no difference in T_1 value was found. Overall the values of dGEMRIC indexed *in vivo* in this study fell within the range of 400-900 ms which has been found in previous work[24].

Patterns of artifact in the phantom T_1 maps with metal present varied with phantom material and sequence (IR, SR, IR-MARS, SR-MARS). The pattern of IR artifact was different with the agarose-based phantom than with previous work done with a saline-based phantom (Figure 1). While neither material adequately represents cartilage tissue, it seems clear that many factors affect the location of artifact, and each imaging

set-up should be evaluated individually. Area of artifact was larger with the IR sequence than the SR sequence, and reduced somewhat when MARS was added to either sequence. In the phantom T_1 maps, the artifact area tended to include values above the actual T_1 of the agarose, with some especially high values in the IR map (Figure 3).

Differences in T_1 value between small ROIs within a phantom and within ROIs between phantoms may be partly explained by having two separate phantoms that were made with gel rather than liquid. The phantoms were made from the same batch of doped agarose, but because they were necessarily different phantoms, and because we expect the gadolinium to be less mobile in the gel, differences in T_1 between the phantoms and between different locations in a phantom may be expected. It is not clear how large an effect this might have on T_1, or what other factors may be involved. Differences in the away ROIs were less than 6% within phantoms, and less than 19% between phantoms.

Our results suggest that a number of factors must be considered when choosing between SR and IR sequences for dGEMRIC and when comparing dGEMRIC results using these sequences. It is clear from the smaller extent of artifacts that SR is more robust than IR in the presence of B_1 inhomogeneity. However SR suffers from limitations in SNR.

The changes of 10% or less in ROI_{away1} and ROI_{away2} in the IR series with metal (MARS and no MARS) are around or below the level of typical clinical significance (examples from literature show differences between groups in the range of 7% to 20%[6,8,10]). The differences may be partly due to using two different phantoms, with potential spatial variations in gadolinium concentration. We expect that outside of the artifact area, the

values will be stable for IR. Determining the extent and direction of artifact will be critical for the application of this technique.

The strengths of this work include the application of several metal artifact reduction strategies both in a phantom and *in vivo* and the use of a relevant surgical implant. One limitation of this work is that few subjects with titanium osteotomy plates have been available for imaging *in vivo*, which has limited our subject numbers, although imaging more than one joint compartment in each subject mitigates this somewhat because we are able to consider cartilage in various loading environments and with varying levels of artifact. A second limitation is that MARS corrects for mis-mapping in the imaging plane, but does not affect mis-mapping of signal into adjacent slices. New protocols for metal artifact correction are now available, and may improve the use of dGEMRIC with surgical hardware[31,32]. We have also used a titanium implant, where stainless steel is the clinical standard. With this type of surgery and hardware, we were unable to obtain any cartilage information near a stainless steel implant. This limits the applicability of this work in this particular population to patients receiving titanium implants. Subject motion, especially motion through the imaging plane, may introduce error into T_1 maps. While planar registration of images can correct in-plane motion, out-of-plane motion is not correctable with 2D dGEMRIC images.

dGEMRIC in the presence of surgical hardware at 3 Tesla may be possible with some appropriately applied strategies. Titanium hardware rather than stainless steel is essential for imaging near metal. Implanted surgical hardware may produce artifacts in T_1 maps used for dGEMRIC that are not obvious on the images used to generate these maps. Depending on the proximity of the cartilage to the hardware and other factors, the artifact may or may not extend into the cartilage. For implanted hardware where the

artifact does not extend through the cartilage, the IR series with MARS provides results consistent with the original (no metal) values within 10%. For experimental situations where the IR artifact extends into the cartilage (shifted null point curves and low f values are obtained), the SR series with MARS has a much smaller area of artifact, though its larger variability may preclude finding smaller clinically significant changes. Using these modified dGEMRIC approaches may allow investigators to study the effects of some surgical procedures on cartilage longitudinally. Caution is advised, however, as the specifics of each implant and imaging experiment set-up influence the extent of artifact and the interference in obtaining reliable dGEMRIC values, and should be evaluated individually.

Conflict of Interest

The authors declare that they have no conflict of interest.

Acknowledgements

This study was supported by a Canadian Institutes for Health Research (CIHR) Operating grant, a Natural Sciences and Engineering Research Council (NSERC) Collaborative Health Research Projects grant, a Michael Smith Foundation Trainee Award (AGD), a Natural Sciences and Engineering Research Council (NSERC) Post Graduate Fellowship (AGD), and a Canadian Arthritis Network Scholarship (DRW).

References

1. Bashir A, Gray ML, Hartke J, Burstein D. Nondestructive imaging of human cartilage glycosaminoglycan concentration by MRI. Magn Reson Med. 1999;41:857–65.

2. Kurkijärvi JE, Nissi MJ, Kiviranta I, Jurvelin JS, Nieminen MT. Delayed gadolinium-enhanced MRI of cartilage (dGEMRIC) and T2 characteristics of human knee articular cartilage: topographical variation and relationships to mechanical properties. Magn Reson Med. 2004;52:41–6.

3. Burstein D, Velyvis J, Scott KT, Stock KW, Kim YJ, Jaramillo D, et al. Protocol issues for delayed Gd(DTPA)(2-)-enhanced MRI (dGEMRIC) for clinical evaluation of articular cartilage. Magn Reson Med. 2001;45:36–41.

4. Gillis A, Bashir A, McKeon B, Scheller A, Gray ML, Burstein D. Magnetic resonance imaging of relative glycosaminoglycan distribution in patients with autologous chondrocyte transplants. Invest Radiol. 2001;36:743–8.

5. Kurkijärvi JE, Mattila L, Ojala RO, Vasara a I, Jurvelin JS, Kiviranta I, et al. Evaluation of cartilage repair in the distal femur after autologous chondrocyte transplantation using T2 relaxation time and dGEMRIC. Osteoarthritis and cartilage / OARS, Osteoarthritis Research Society. 2007 Apr;15:372–8.

6. Tiderius CJ, Svensson J, Leander P, Ola T, Dahlberg L. dGEMRIC (delayed gadolinium-enhanced MRI of cartilage) indicates adaptive capacity of human knee cartilage. Magn Reson Med. 2004;51:286–90.

7. Roos EM, Dahlberg L. Positive effects of moderate exercise on glycosaminoglycan content in knee cartilage: a four-month, randomized, controlled trial in patients at risk of osteoarthritis. Arthritis and rheumatism. 2005 Nov;52:3507–14.

8. Williams A, Sharma L, McKenzie CA, Prasad P V, Burstein D. Delayed gadolinium-enhanced magnetic resonance imaging of cartilage in knee osteoarthritis: findings at different radiographic stages of disease and relationship to malalignment. Arthritis Rheum. 2005 Nov;52:3528–35.

9. Nojiri T, Watanabe N, Namura T, Narita W, Ikoma K, Suginoshita T, et al. Utility of delayed gadolinium-enhanced MRI (dGEMRIC) for qualitative evaluation of articular cartilage of patellofemoral joint. Knee Surg Sports Traumatol Arthrosc. 2006 Aug;14:718–23.

10. Tiderius CJ, Olsson LE, Nyquist F, Dahlberg L. Cartilage glycosaminoglycan loss in the acute phase after an anterior cruciate ligament injury: Delayed gadolinium-enhanced magnetic resonance imaging of cartilage and synovial fluid analysis. Arthritis Rheum. 2005;52:120–7.

11. Owman H, Tiderius CJ, Neuman P, Nyquist F, Dahlberg LE. Association between findings on delayed gadolinium-enhanced magnetic resonance imaging of cartilage and future knee osteoarthritis. Arthritis Rheum. 2008 Jun;58:1727–30.

12. Tiderius CJ, Olsson LE, Leander P, Ekberg O, Dahlberg L. Delayed gadolinium-enhanced MRI of cartilage (dGEMRIC) in early knee osteoarthritis. Magn Reson Med. 2003;49:488–92.

13. Yamashita T, Watanabe A, Ochiai S, Matsuki K, Kamikawa K, Toyone T, et al. Time course evaluation of extracellular matrix after high tibial osteotomy using delayed gadolinium enhanced MR imaging of cartlage. Osteoarthritis Research Society International; 2008. p. Abstract 415.

14. Young AA, Stanwell P, Williams A, Rohrsheim JA, Parker DA, Giuffre B, et al. Glycosaminoglycan Content of Knee Cartilage Following Posterior Cruciate Ligament Rupture Demonstrated by Delayed Gadolinium-Enhanced Magnetic Resonance Imaging of Cartilage (dGEMRIC). J Bone Joint Surg Am. 2005;87-A:2763–8.

15. Parker DA, Beatty KT, Giuffre B, Scholes CJ, Coolican MRJ. Articular cartilage changes in patients with osteoarthritis after osteotomy. The American journal of sports medicine. 2011 May;39:1039–45.

16. Rutgers M, Bartels LW, Tsuchida AI, Castelein RM, Dhert WJ, Vincken KL, et al. dGEMRIC as a tool for measuring changes in cartilage quality following high tibial osteotomy: a feasibility study. Osteoarthritis and cartilage / OARS, Osteoarthritis Research Society. Elsevier Ltd; 2012 Oct;20:1134–41.

17. Kolind SH, MacKay AL, Munk PL, Xiang QS. Quantitative evaluation of metal artifact reduction techniques. J Magn Reson Imaging. 2004;20:487–95.

18. Chang SD, Lee MJ, Munk PL, Janzen DL, MacKay A, Xiang QS. MRI of spinal hardware: comparison of conventional T1-weighted sequence with a new metal artifact reduction sequence. Skeletal radiology. 2001 Apr;30:213–8.

19. Lee MJ, Janzen DL, Munk PL, MacKay A, Xiang QS, McGowen A. Quantitative assessment of an MR technique for reducing metal artifact: application to spin-echo imaging in a phantom. Skeletal radiology. 2001 Jul;30:398–401.

20. Olsen R V., Munk PL, Lee MJ, Janzen DL, MacKay AL, Xiang QS, et al. Metal artifact reduction sequence: early clinical applications. Radiographics. 2000;20:699–712.

21. Norris D. Adiabatic radiofrequency pulse forms in biomedical nuclear magnetic resonance. Concepts in Magnetic Resonance. 2002;14:89–101.

22. Kim Y-J, Jaramillo D, Millis MB, Gray ML, Burstein D. Assessment of early osteoarthritis in hip dysplasia with delayed gadolinium-enhanced magnetic resonance imaging of cartilage. The Journal of bone and joint surgery. American volume. 2003 Oct;85-A:1987–92.

23. Cho ZH, Kim DJ, Kim YK. Total inhomogeneity correction including chemical shifts and susceptibility by view angle tilting. Medical physics. 1988;15:7–11.

24. McKenzie CA, Williams A, Prasad P V, Burstein D. Three-dimensional delayed gadolinium-enhanced MRI of cartilage (dGEMRIC) at 1.5T and 3.0T. Journal of magnetic resonance imaging : JMRI. 2006 Oct;24:928–33.

25. White LM, Buckwalter KA. Technical considerations: CT and MR imaging in the postoperative orthopedic patient. Semin Musculoskelet Radiol. 2002;6:5–17.

26. Eustace S, Goldberg R, Williamson D, Melhem ER, Oladipo O, Yucel EK, et al. MR imaging of soft tissues adjacent to orthopaedic hardware: techniques to minimize susceptibility artefact. Clin Radiol. 1997 Aug;52:589–94.

27. Lee M, Kim S, Lee S, Song H, Huh Y, Kim D, et al. Overcoming Artifacts from Metallic Orthopedic Implants at High-Field-Strength MR Imaging and Multi-detector CT. Radiographics. 2007;27:791–804.

28. Harris CA, White LM. Metal artifact reduction in musculoskeletal magnetic resonance imaging. Orthop Clin North Am. 2006 Jul;37:349–59, vi.

29. Suh JS, Jeong EK, Shin KH, Cho JH, Na JB, Kim DH, et al. Minimizing artifacts caused by metallic implants at MR imaging: experimental and clinical studies. AJR Am J Roentgenol. 1998;171:1207–13.

30. Laakman RW, Kaufman B, Han JS, Nelson AD, Clampitt M, O'Block AM, et al. MR imaging in patients with metallic implants. Radiology. 1985 Dec;157:711–4.

31. Koch KM, Busse RF, Lewein TA, Potter HG, Hinks RS, King KF. Multiple Resonant Frequency Offset Acquisitions for Imaging of Metallic Implants. The International Society for Magnetic Resonance in Medicine, Toronto. 2008. p. 1250.

32. Lu W, Pauly KB, Gold GE, Pauly JM, Hargreaves BA. SEMAC: Slice Encoding for Metal Artifact Correction in MRI. Magn Reson Med. 2009 Jul;62:66–76.

FIGURE CAPTIONS

Figure 1: Photo of phantom (a), with arrow indicating direction of B_0 field and head direction, and (b) definition of ROIs on a TI = 50 ms image, where each rectangle is an ROI containing 900 pixels, labeled with the ROI name. (c) TI = 50 ms image and inset photo of saline phantom showing different pattern of artifact in image compared to agarose gel phantom, using same sequence parameters.

Figure 2: IR images (left, center) of subjects with high tibial osteotomy implants, and T_1 map (right) from images with titanium (arrow indicates demarcation which indicates the presence of an artifact not apparent in the image). Below, single pixel curves from outside (left) and within (right) the artifact (location of pixels denoted by crosshairs).

Figure 3: T_1 maps of IR and SR phantom studies with metal, with and without MARS. The white rectangles outline the small ROIs defined in Figure 1.

Figure 4: f-maps and M_0-maps of IR and SR phantom studies with metal, with and without MARS. The extent of artifact is clearer in the f-maps for IR-based series, while the M_0-maps show the extent of artifact better for SR-based series. The white rectangles outline the small ROIs defined in Figure 1.

Figure 5: Histograms of phantom studies with and without metal, and with and without MARS (including outliers). Dotted lines indicate the position of largest bin for IR and SR respectively in the 'no metal, no MARS' condition.

Figure 6: IR images at TI = 1800 ms (left) and TI = 50 ms (centre) of phantom with metal plate and screws. The dark lines around the artifact edges indicate lines of constant B_1 (assuming constant T_1 in phantom) which gave rise to a null point at that TI time. Right, eight single pixel curves (spaced every four pixels) showing the change in values within the dark-line artifact (position of pixels indicated by colours; arrows indicate direction from outside artifact across dark line).

Figure 7: T_1 maps of the same patellofemoral joint (axial) using IR and SR (top left and right). Images were taken two days apart. T_1 maps of the same tibiofemoral joint (lateral compartment, coronal) using IR, SR and SR-MARS (middle left, center and right). The SR-MARS image was taken eleven months later, however it was statistically compared to an SR image taken at the same time. A single pixel result from the TF IR map (location bottom left) shows the same shifted null point (bottom centre), and a disruption in the f_{IR} map (bottom right) with values far below the nominal $f_{IR} = 2$.

Table 1: MRI sequence parameters for all sequences.

	IR	SR	IR-MARS	SR-MARS
Repetition time (TR)	2200 ms	1800, 1200, 700, 400, 300, 200, 150, 100 ms	2200 ms	1800, 1200, 700, 400, 300, 200, 150, 100 ms
Inversion time (TI)	1800, 1200, 700, 400, 200, 150, 100, 50 ms	-	1800, 1200, 700, 400, 200, 150, 100, 50 ms	-
Echo time (TE)	15 ms	15 ms	15 ms	15 ms
TSE factor	9	2	9	2
Field of view (FOV)	100 mm	100 mm	100 mm	100 mm
Slice thickness	3 mm	3 mm	3 mm	3 mm
Matrix size (scanned)	256 x 256	256 x 256	256 x 256	256 x 256
Matrix size (reconstructed)	256 x 256	256 x 256	256 x 256	256 x 256
In-plane resolution	0.39 x 0.39 mm	0.39 x 0.39 mm	0.39 x 0.39 mm	0.39 x 0.39 mm
Number of slices	1	1	1	1
Scan time (total)	16:25	12:53	16:25	12:53
VAT	No	No	Yes	Yes
Bandwidth	+/- 26.9 kHz	+/- 26.9 kHz	+/- 46.0 kHz	+/- 46.0 kHz

Table 2

Table 2 Results from ROI analyses of phantom and *in vivo* T_1 maps. $ROI_{artifact}$ contained many outliers (pixels outside 100-1200 ms range) in the IR scans, so $ROI_{artifact}$ T_1 results with outliers included (all 900 pixels) are also presented.

Phantom results	No. of included pixels/outlier pixels in image	Mean (SD) all pixels [ms]	Mean (SD) $ROI_{cartilate}$ [ms]	Mean (SD) ROI_{away1} [ms]	Mean (SD) ROI_{away2} [ms]	No. of included pixels/ outlier pixels in $ROI_{artifact}$	Mean (SD) $ROI_{artifact}$ [ms]	Mean (SD) $ROI_{artifact}$ [ms] Incl. outlier pixels
IR, no metal	65430/106	569.7 (25.1)	541.0 (9.4)	600.1 (11.5)	541.8 (10.6)	900/0	594.7 (10.8)	594.7 (10.8)
SR, no metal	65430/106	538.6 (26.7)	520.7 (18.4)	545.0 (21.1)	502.9 (19.3)	900/0	561.2 (18.7)	561.3 (18.7)
IR-MARS, no metal	65430/106	568.4 (26.7)	540.7 (12.3)	597.1 (15.3)	537.7 (12.7)	900/0	594.5 (13.3)	594.5 (13.3)
SR-MARS, no metal	65430/106	550.3 (31.3)	533.6 (25.2)	575.2 (31.1)	514.8 (24.1)	900/0	568.0 (22.7)	568.0 (22.7)
IR, metal	57343/8193	606.9 (97.7)	601.7 (43.9)	561.0 (10.8)	594.8 (10.8)	552/348	675.8 (206.8)	1491.2 (1180.6)
SR, metal	59185/6351	616.8 (104.8)	616.2 (48.3)	565.5 (25.9)	596.9 (26.5)	896/4	635.6 (58.6)	638.9 (77.1)
IR-MARS, metal	55871/9665	606.7 (90.5)	595.4 (24.7)	563.7 (14.6)	595.8 (13.7)	527/373	597.7 (234.5)	1396.0 (1266.0)
SR-MARS, metal	58540/6996	613.1 (112.8)	589.7 (52.1)	539.1 (31.4)	559.9 (30.1)	900/0	606.5 (43.6)	606.5 (43.6)

***In vivo* results**	No. of included pixels/outlier pixels in ROI	Mean (SD) [ms]	Mean (SD) incl. outlier pixels [ms]	Imaging timeline
PF IR	854/2	547 (133)	549 (139)	0
PF SR	896/7	596 (177)	604 (212)	2 days
TF IR	891/7	436 (116)	448 (187)	2 days
TF SR	830/112	486 (212)	730 (769)	0
TF SR	811/24	546 (164)	585 (313)	11 months
TF SR-MARS	839/77	589 (205)	720 (543)	11 months

Table 3 Results from noise level simulation (900 noisy data sets fitted and averaged for each noise level and T_1 measurement type). Nominal values of T_1, M_0 and f were taken from curve fit results for the separate IR and SR 'no metal, no MARS' phantom data. For these results, a random set of 25 initial values of T_1 and SI were used for each noisy data set, and the solution with the lowest norm of residual was selected as the best result for that set.

Signal to noise ratio (SNR)	Average calc. T_1 IR [ms]	SD T_1 IR [ms]	Average calc. T_1 SR [ms]	SD T_1 SR [ms]
Infinity	570.00	> 0.01	537.00	> 0.01
1000	568.98	1.20	537.07	2.37
100	568.98	12.52	537.80	23.67
50	568.99	24.69	541.27	48.07
30	567.00	39.43	549.09	83.73
20	561.02	63.73	570.00	139.28
18	565.48	81.32	568.28	150.24
15	580.46	120.17	590.50	192.08
12	568.37	139.87	607.52	240.81
10	578.40	173.63	621.50	268.89
9	587.79	197.87	625.77	289.44
8	597.06	223.35	644.19	308.92
7	608.50	253.99	670.51	340.76
6	610.10	271.99	701.82	367.44
5	605.16	288.57	713.97	388.65

Figure 1

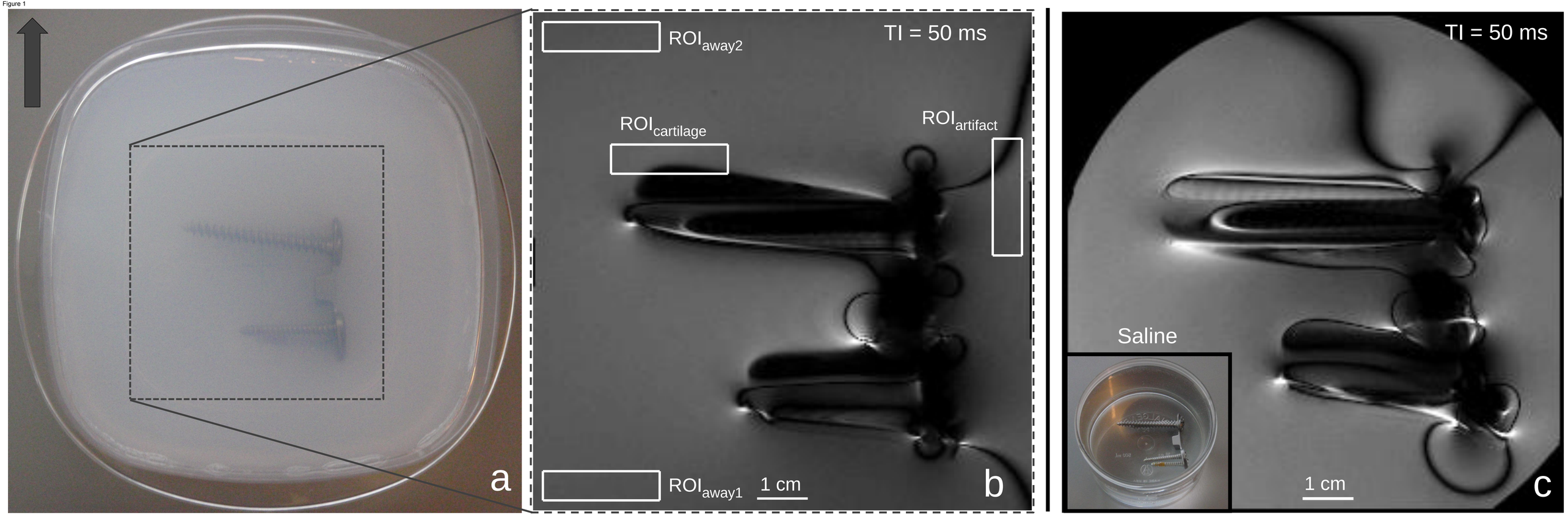
a
ROI away2
TI = 50 ms
ROI cartilage
ROI artifact
ROI away1
1 cm
b
TI = 50 ms
Saline
1 cm
c

Figure 2
Click here to download high resolution image

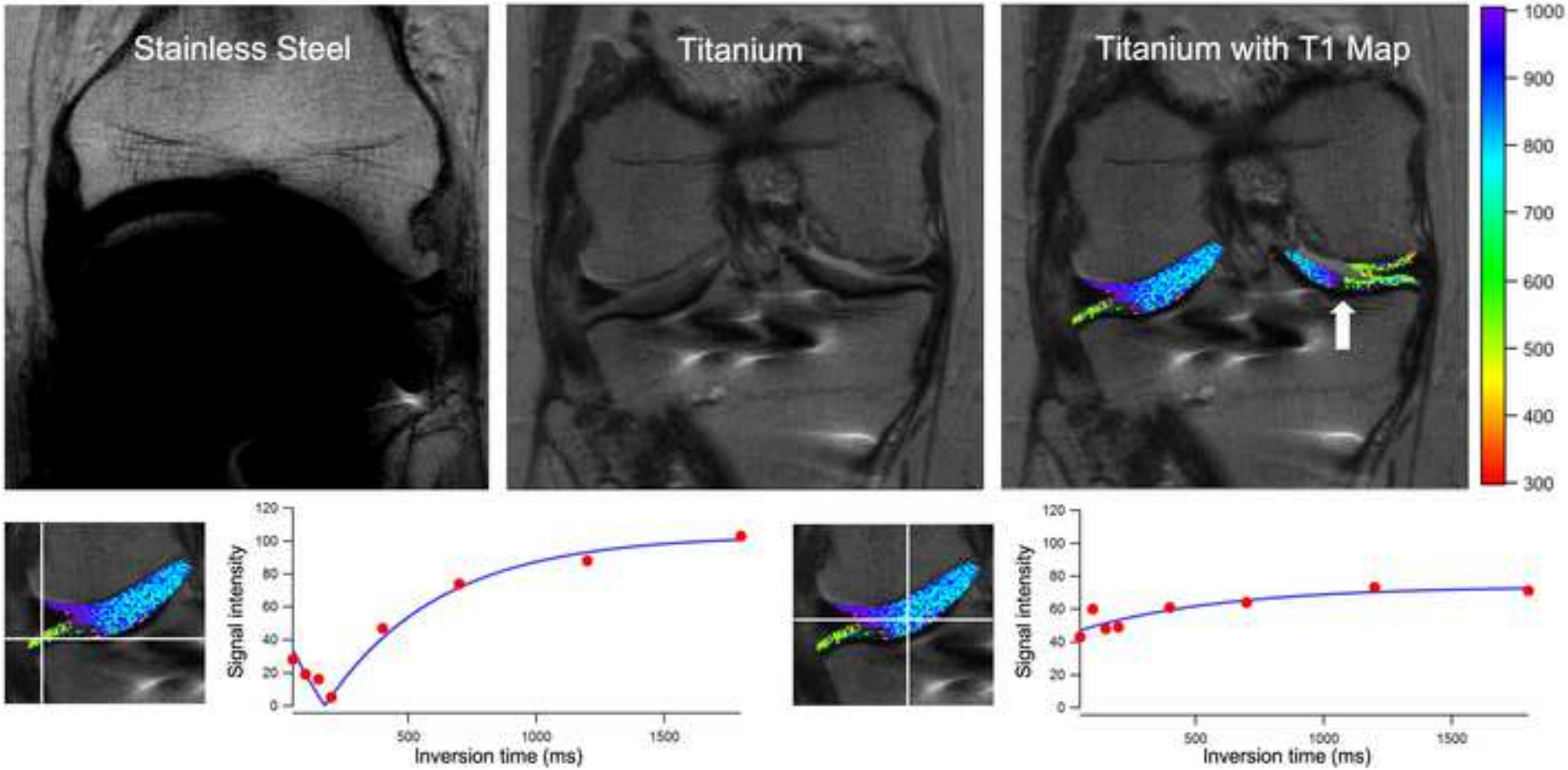

Figure 3

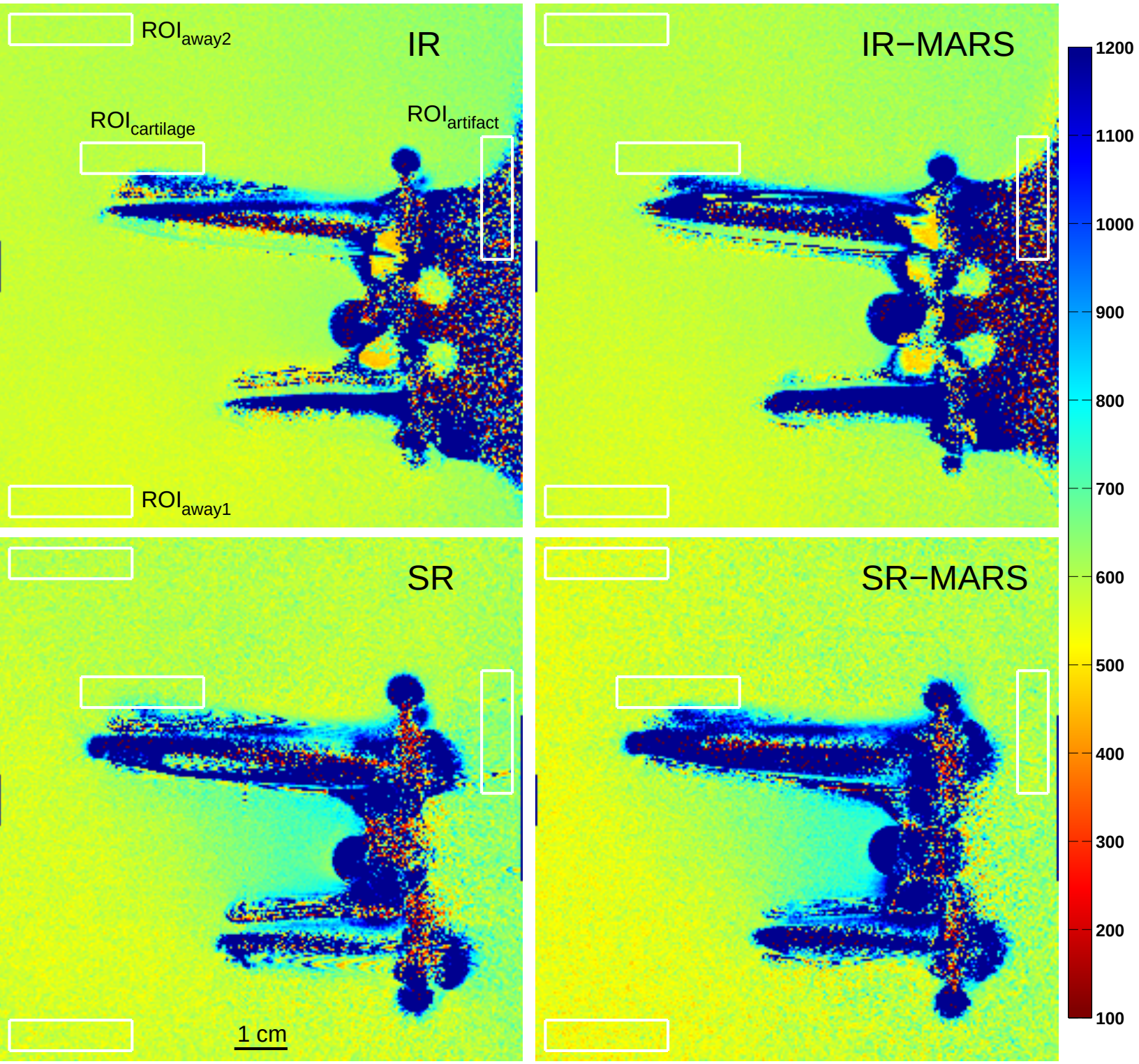
ROI away2
IR
ROI cartilage
ROI artifact
ROI away1
IR−MARS
SR
1 cm
SR−MARS
1200
1100
1000
900
800
700
600
500
400
300
200
100

Figure 4
Click here to download high resolution image

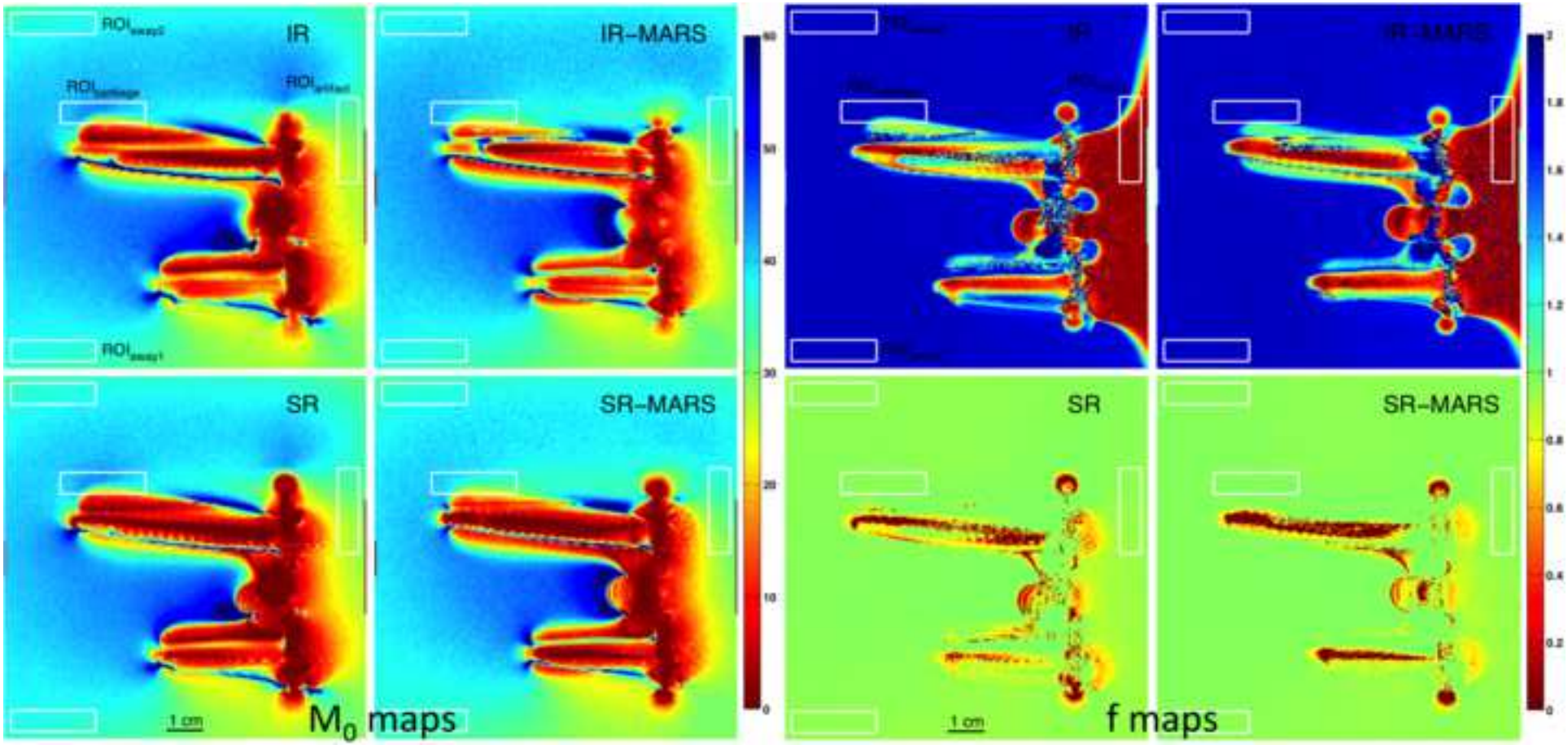

Figure 5

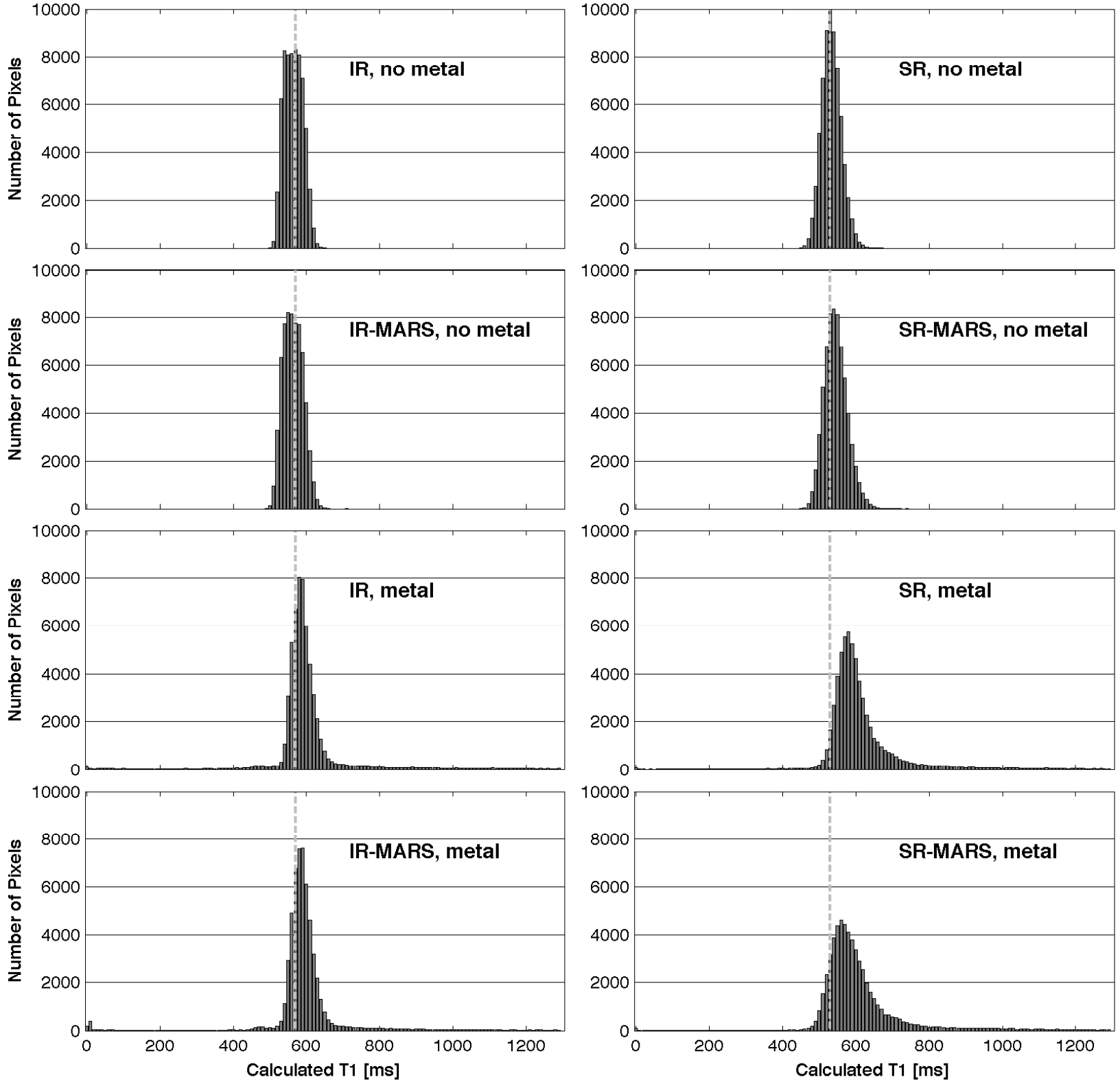
IR, no metal
SR, no metal
IR-MARS, no metal
SR-MARS, no metal
IR, metal
SR, metal
IR-MARS, metal
SR-MARS, metal
Number of Pixels
Calculated T1 [ms]
0
2000
4000
6000
8000
10000
0
200
400
600
800
1000
1200

Figure 6

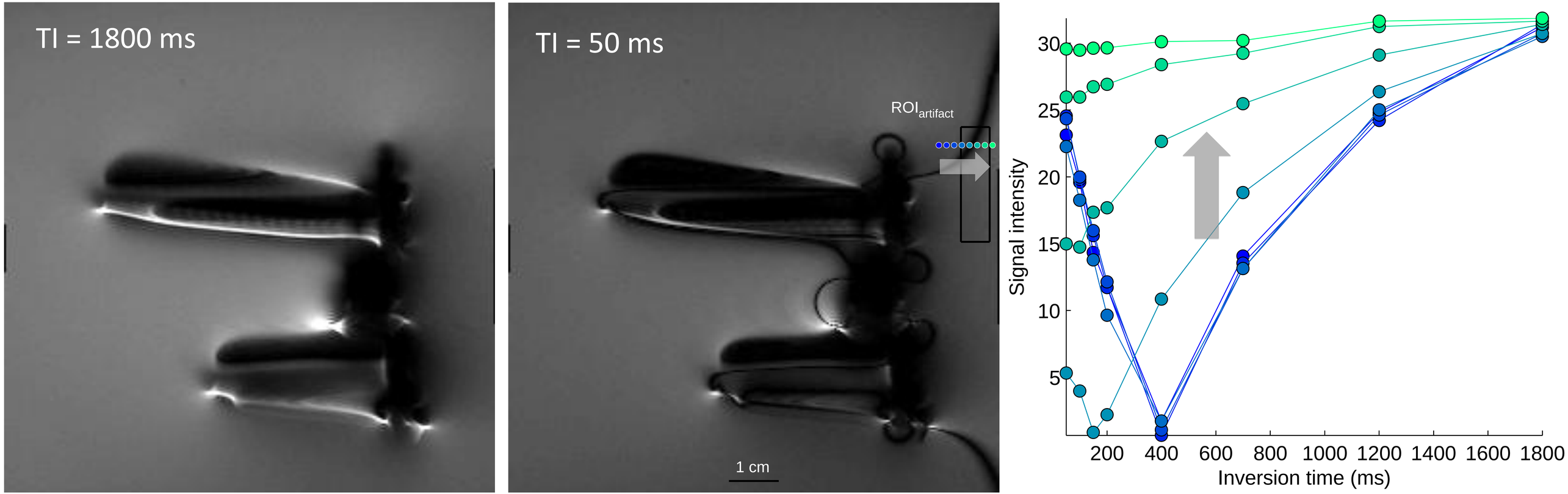
TI = 1800 ms
TI = 50 ms
ROI artifact
1 cm
Signal intensity
30
25
20
15
10
5
200
400
600
800
1000
1200
1400
1600
1800
Inversion time (ms)

Figure 7

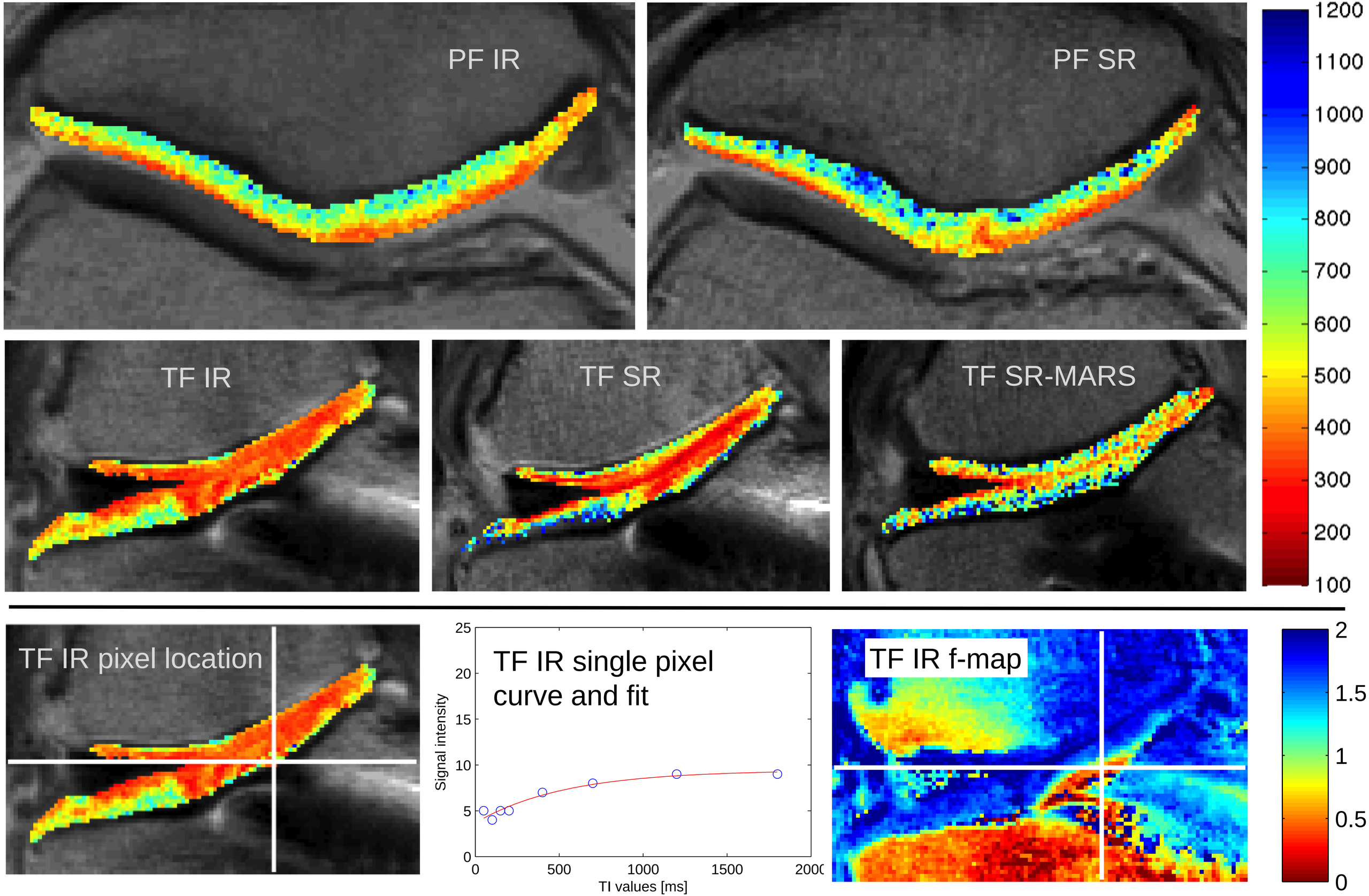
PF IR
PF SR
TF IR
TF SR
TF SR-MARS
1200
1100
1000
900
800
700
600
500
400
300
200
100
TF IR pixel location
TF IR single pixel curve and fit
Signal intensity
TI values [ms]
0
500
1000
1500
2000
0
5
10
15
20
25
TF IR f-map
2
1.5
1
0.5
0